Modeling of Solid-Bowl Batch Centrifugation of Flocculated Suspensions

Anthony D. Stickland
Particulate Fluids Processing Special Research Centre, Dept. of Chemical and Biomolecular Engineering, The University of Melbourne, Victoria, Australia, 3010

Lee R. White
Centre for Complex Fluid Engineering, Dept. of Chemical Engineering, Carnegie Mellon University, Pittsburgh, PA 15213

Peter J. Scales
Particulate Fluids Processing Special Research Centre, Dept. of Chemical and Biomolecular Engineering, The University of Melbourne, Victoria, Australia, 3010

DOI 10.1002/aic.10746
Published online December 12, 2005 in Wiley InterScience (www.interscience.wiley.com).

Solid-bowl batch centrifuges are used to thicken particulate and flocculated suspensions in many varied applications. The volume fraction dependent material parameters of compressive yield stress and hindered settling function are used to describe the solid-liquid separation of a two-phase system caused by centrifugal acceleration. The solution of the transient conservation of momentum and mass equations in radial coordinates gives the volume fraction distribution as a function of time for the two cases of the initial suspension networked or un-networked. Analytical solutions are given for the equilibrium distribution and the small-scale time dependence. The governing equations for the transient behaviors are solved using a 4^{th}-5^{th} order Runge-Kutta adaptive step-size numerical method. The results show three zones of behavior: a consolidating bed, a sedimentation zone, and a clear-liquor zone. The volume fraction within the sedimentation zone is constant for the initially networked case, and constant with radius but diminishing with time for the initially un-networked case. © 2005 American Institute of Chemical Engineers
AIChE J, 52: 1351–1362, 2006
Keywords: solid-liquid separation, solid-bowl batch centrifugation, consolidation, sedimentation, thickening, flocculated suspensions, Runge-Kutta numerical method

Introduction

Centrifuges are used extensively by many industries to perform solid-liquid separation, from dewatering biosludges in wastewater treatment to performing delicate protein separation. In two-phase systems, the centrifugal buoyancy due to the phase density difference causes the solids to thicken against the bowl of the centrifuge. There are two basic types: thickening and filtering centrifuges (the centrifugal analogies for gravity thickening and gravity filtration, respectively), which can be operated in batch, semi-continuous, or continuous modes.

In thickening centrifuges, the bowl wall is solid: the particles settle against the wall of the centrifuge and form a cake, and the liquor is withdrawn from above the cake. *Disc*, *decanter*, and *tubular* centrifuges are examples of thickening centrifuges. Disc centrifuges have internal conical discs to aid sedimenta-

Correspondence concerning this article should be addressed to P. J. Scales at peterjs@unimelb.edu.au.

tion, which is analogous to the use of lamella plates in gravity thickening. Decanter centrifuges use an internal screw or scroll that rotates at a different speed to the bowl to push the cake through the centrifuge. The distinction is made between solid-bowl tubular centrifuges, where a radial coordinate is required, and laboratory tube centrifuges, where a Cartesian coordinate with radial acceleration is used.

In filtering centrifuges, the bowl wall is semipermeable, and the liquor is drawn through the cake and out the walls of the centrifuge. *Pendulum*, *pusher*, and *knife* centrifuges are examples of filtering centrifuges.

The first tubular centrifuge models were based upon the Stokes settling trajectory of a particle of a given size, called Sigma Theory.[1,2] It was acknowledged but not considered that the consolidation of the solid phase under centrifugal acceleration critically affected the efficiency of the centrifuge. Conventional filtration theory was expanded to include the effect of liquid flow through a consolidating cake using Darcy's law[3] and applied to centrifugal thickening by Tiller and Hysung.[4] A correction factor was introduced into Sigma Theory to include this effect,[5] but it is not useful for highly compressible materials. Anestis and Schneider[6] extended Kynchian theory[7] based on the theory of kinematic waves to one-dimensional batch centrifugation in radial coordinates and showed that the sediment concentration is a function of time for ideal suspensions.

Buscall and White[8] developed a phenomenological theory of solid-liquid separation in which the behavior of a particulate network in compression is determined by the local solids volume fraction, ϕ, dependent parameters of compressive yield stress, $p_y(\phi)$, and hindered settling function, $R(\phi)$. Green et al.[9] used this approach to model the equilibrium state of a consolidated suspension in a centrifugal tube (that is, a Cartesian coordinate problem with centrifugal acceleration). The theory has also been used to model the transient batch[10] and steady-state continuous[11] settling of a suspension under gravitational acceleration, one-dimensional (1-D) constant pressure filtration,[12-14] and 1-D gravity filtration.[15] Filtration, sedimentation, and centrifugation techniques for determining the local material properties have been developed based upon these theories.[9,16,17]

In this work, the solid-liquid separation performed by batch-thickening centrifugation is modeled by formulating the mass and momentum conservation equations into radial coordinates with centrifugal acceleration, applying appropriate scalings, and identifying the boundary conditions for each zone. Analytical solutions are used to give the equilibrium distribution and the small-scale time dependence. The governing equations for the transient behaviors are solved using a forward difference approximation in time and an iterative 4^{th}-5^{th} order Runge-Kutta adaptive step-size numerical method in the spatial direction.

The solution is dependent on the initial solids concentration, ϕ_0, relative to the gel point, ϕ_g, where ϕ_g is the solids volume fraction at which a network forms (thus, there is no measurable network strength at concentrations below ϕ_g). Models are presented for both the initial suspension networked ($\phi_0 > \phi_g$) and the initial suspension un-networked ($\phi_0 < \phi_g$) cases. The conservation equations given here are analogous to the formulations of Bürger and Concha,[18] who incorporated a similar phenomenological approach for the $\phi_0 < \phi_g$ case to extend the work of Anestis and Schneider[6] to include cake compression.

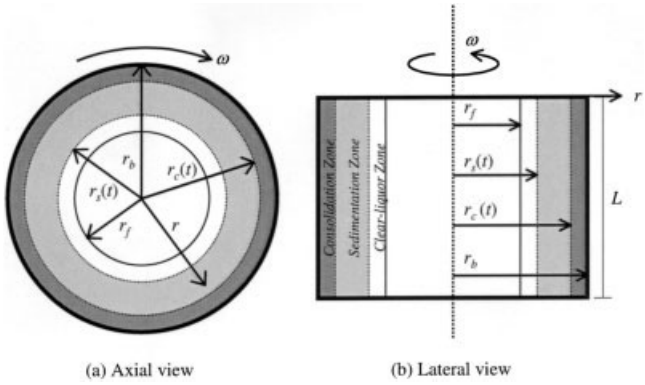

Figure 1. One-dimensional solid-bowl centrifugal thickening.

(a) Axial view, (b) lateral view.

This work does not consider the effects of internal discs, as seen in disc-bowl centrifuges, or continuous or semi-continuous operation. Likewise, models of filtering centrifuges must consider the reducing applied pressure due to the falling head of fluid, the resistance of the membrane, and the capillary-assisted cake compaction caused by fluid drainage, and are also not considered further here.[19,20]

Theory

Solid-bowl batch centrifugation

Axial and lateral views of 1-D solid-bowl batch centrifugation are presented in Figure 1. At the start of the process ($t = 0$), the sludge is assumed uniform at a concentration of ϕ_0. The centrifuge spins at constant angular velocity, ω. The centrifugal action exerts acceleration upon the particles and thickening begins. Three zones of behavior are distinguishable:

– A consolidation zone of material at concentrations greater than ϕ_g (or greater than ϕ_0 in the $\phi_0 > \phi_g$ case) forms against the bowl of the centrifuge ($r = r_b$). A network of particles exists where the local stress on the network, p_p, is equal to the compressive yield stress of the network, $p_y(\phi)$;

– A sedimentation zone exists where the particles are in free-fall. The sediment behaves differently for the networked and un-networked cases[11]:

- For the $\phi_0 > \phi_g$ case, a network exists but the consolidating forces are less than the compressive yield stress, so the zone slumps at a constant concentration. The network is able to transmit pressure, which varies from 0 at the top of the sediment, $r_s(t)$, to $p_y(\phi_0)$ at the boundary between the sedimentation and consolidation zones, $r_c(t)$. $\phi(r,t)$ is continuous so that $\phi\ (r_c^+,t) = \phi_0$. At equilibrium, the sedimentation zone still exists, since the compressive forces do not surpass $p_y(\phi_0)$ for $r < r_c(\infty)$.
- For the $\phi_0 < \phi_g$ case, no network exists in the sedimentation zone and the particle velocity is independent of $p_y(\phi)$. In one-dimensional centrifugal thickening with a constant cross section, the sedimentation zone remains at a constant concentration, ϕ_0.[9] However, in radial coordinates, the increasing area has the effect of thinning the sediment, such that the volume fraction in the sedimentation zone, $\phi_s(t)$, is a function of time. $r_c(t)$ is discontinuous, with the volume fraction at the top of the

bed $\phi(r_c^+,t) = \phi_g$ and, just above the bed, $\phi(r_c^-,t) = \phi_s(t)$. A critical time, t_c, exists when $r_c(t)$ is equal to $r_s(t)$, that is, when all of the particles have settled to the consolidating bed and the sedimentation zone vanishes. After t_c, the boundary at r_c remains discontinuous, with $\phi(r_c^+,t) = \phi_g$ and $\phi(r_c^-,t) = 0$. The bed compresses until the equilibrium state is reached.

– The third zone is the clear-liquor zone from which solid material has settled ($\phi = 0$). r_f is the fluid height, which is determined from the initial volume of suspension per unit drum length, V_0:

$$r_f = \sqrt{r_b^2 - \frac{V_0}{\pi}} \tag{1}$$

Sedimentation-consolidation equations

The compressional rheology model of solid-liquid separation developed by Buscall and White[8] balances the hydrodynamic, hydrostatic, particle pressure, and acceleration (gravitational or centrifugal) forces acting upon a volume element of solids to obtain the momentum conservation equations for the solid and liquid phases. Eliminating the fluid pressure gradient gives the momentum conservation equation for the suspension in vector notation:

$$-\frac{\phi}{1-\phi} R(\phi)(\mathbf{u} - \mathbf{w}) - \nabla p_p + \phi \Delta\rho \mathbf{g} = 0 \tag{2}$$

$R(\phi)$ is the hydrodynamic drag coefficient at volume fraction ϕ, $\boldsymbol{u} - \mathbf{w}$ is the local velocity of the particle relative to the fluid, p_p is the local particle pressure, $\Delta\rho$ is the density difference between the solid and liquid phases, and $\mathbf{g}$ is the acceleration vector. The first term in Eq. 2 represents the drag due to the fluid-solid interaction; the second term is the force on the solids due to a solids pressure gradient, while the third term represents the solids weight. The assumption is made that the shear stresses are negligible.

The conservation of mass equation for the particle phase is:

$$\frac{\partial \phi}{\partial t} = -\nabla \cdot (\phi \mathbf{u}) \tag{3}$$

The conservation of suspension volume is:

$$\nabla \cdot (\phi \mathbf{u} + (1-\phi)\mathbf{w}) = 0 \tag{4}$$

In 1-D radial coordinates with $\mathbf{u} = u(r,t)$ and $\mathbf{w} = w(r,t)$, Eq. 4 is:

$$\frac{1}{r}\frac{\partial}{\partial r}[r(\phi u + (1-\phi)w)] = 0 \tag{5}$$

Integrating Eq. 5 with respect to r and equating to zero since the total volume is conserved for batch thickening gives:

$$w = -\frac{\phi}{(1-\phi)} u \tag{6}$$

Converting Eq. 2 to a one-dimensional radial coordinate with centrifugal acceleration, $\mathbf{g} = \omega^2 r$, and substituting Eq. 6 gives:

$$-\frac{R(\phi)}{(1-\phi)^2}\phi u - \frac{\partial p_p}{\partial r} + \phi \Delta\rho \omega^2 r = 0 \tag{7}$$

If collapse of the particle network due to excess pressure is very rapid compared to the processes of sedimentation and consolidation such that viscous drainage of the suspending fluid rather than bond breakage and re-formation is rate determining (that is, the dynamic compressibility, $\kappa(\phi)$ is very large), the solids pressure can only infinitesimally exceed the network strength.[8,11] The substitution $p_p(r,t) = p_y(\phi(r,t))$ in Eq. 7 yields:

$$-\frac{R(\phi)}{(1-\phi)^2}\phi u - \frac{dp_y(\phi)}{d\phi}\frac{\partial \phi}{\partial r} + \phi \Delta\rho \omega^2 r = 0 \tag{8}$$

The solids continuity equation (Eq. 3) becomes:

$$\frac{\partial \phi}{\partial t} = -\frac{1}{r}\frac{\partial}{\partial r}(r\phi u) \tag{9}$$

These nonlinear partial differential equations (Eqs. 8 and 9) are the overall governing equations for consolidation in solid-bowl batch centrifugal thickening. When combined, they constitute a diffusion equation for $\phi(r,t)$[18] to be solved using the appropriate initial and boundary conditions.

The initial condition is given by the assumption that the sludge concentration is initially uniform at ϕ_0:

$$\phi(r, 0) = \phi_0 \tag{10}$$

The boundary condition at the bowl wall is given by assuming that the bowl wall is impervious, such that the solids velocity is zero:

$$u(r_b, t) = 0 \tag{11}$$

The boundary conditions at $r_c(t)$ and $r_s(t)$ depend on whether the initial suspension is networked or un-networked, and are outlined later. The global conservation of solids volume is:

$$\int_{r_s(t)}^{r_b} r\phi dr = \frac{V_0 \phi_0}{2\pi} \tag{12}$$

Dimensionless equations

The sedimentation-consolidation equations are simplified by applying appropriate scalings. The radial coordinate r is scaled with r_b to give the dimensionless length scale, Z:

$$Z = 1 - \frac{r^2}{r_b^2} \tag{13}$$

Thus, r_b, $r_c(t)$, $r_s(t)$, and r_f map to 0, $Z_c(T)$, $Z_s(T)$, and Z_f, respectively. $p_p(r,t)$ and $p_y(\phi)$ are scaled with the centrifugal force to give $P_p(Z,T)$ and $P_y(\phi)$:

$$P_p(Z, T) = \frac{2}{\Delta\rho\omega^2 r_b^2} p_p(r, t) \tag{14}$$

$$P_y(\phi) = \frac{2}{\Delta\rho\omega^2 r_b^2} p_y(\phi) \tag{15}$$

$R(\phi)$ is scaled with the initial concentration to give $B(\phi)$:

$$B(\phi) = \frac{(1 - \phi_0)^2}{R(\phi_0)} \frac{R(\phi)}{(1 - \phi)^2} \tag{16}$$

Thus, the appropriate time scaling is based on the rate of sedimentation as opposed to the rate of consolidation:

$$T = \frac{2\Delta\rho\omega^2(1 - \phi_0)^2}{R(\phi_0)} t \tag{17}$$

The solids velocity, $u(r,t)$, is scaled to give a dimensionless solids flux, $\psi(Z,T)$:

$$\psi(Z, T) = \frac{R(\phi_0)}{\Delta\rho\omega^2 r_b^2 (1 - \phi_0)^2} r\phi u \tag{18}$$

Substituting these scalings into the governing equations (Eqs. 8 and 9) gives:

$$\frac{\partial\phi}{\partial Z} = -\frac{1}{\Delta(\phi)}\left[\frac{\phi}{B(\phi)} - \frac{\psi}{1 - Z}\right] \tag{19}$$

$$\frac{\partial\psi}{\partial Z} = \frac{\partial\phi}{\partial T} \tag{20}$$

The scaled diffusivity, $\Delta(\phi)$, is defined as:

$$\Delta(\phi) = \begin{Bmatrix} 0 & \phi < \phi_g \\ \dfrac{P_y'(\phi)}{B(\phi)} & \phi \geq \phi_g \end{Bmatrix} \tag{21}$$

The scaled version of Eq. 7 is used when $P_p(Z,T) < P_y(\phi)$:

$$\frac{\partial P_p}{\partial Z} = \frac{B(\phi)}{1 - Z}\psi - \phi \tag{22}$$

The initial condition, wall boundary condition, and global conservation become:

$$\phi(Z, 0) = \phi_0 \tag{23}$$

$$\psi(0, T) = 0 \tag{24}$$

$$\int_0^{Z_s(T)} \phi dZ = Z_f\phi_0 \tag{25}$$

The boundary conditions at $Z_c(T)$ and $Z_s(T)$, and subsequently the method of solution, depend on whether the initial suspension is networked or un-networked. These two cases are now examined separately. In each case, equilibrium and small-time solutions are given and a numerical method for the general time-dependent case is outlined.

Case 1: initial suspension un-networked ($\phi_0 < \phi_g$)

For the $\phi_0 < \phi_g$ case, the particle pressure in the sedimentation zone is zero, since the concentration is below that which is necessary to transmit a stress. The top of the cake is at ϕ_g.

Equilibrium Solution ($\phi_0 < \phi_g$, $T \to \infty$). For large time, all the solids settle from the sedimentation zone in the $\phi_0 < \phi_g$ case. The equilibrium solution, $\phi(Z,\infty)$, is found by setting the time derivatives and the solids flux, ψ, in the consolidation equations to zero. Equation 19 becomes:

$$\frac{d\phi}{dZ} = -\frac{\phi}{P_y'(\phi)} \tag{26}$$

The boundary conditions to this ordinary differential equation are $\phi(0,\infty) = \phi_\infty$ and $\phi(Z_c(\infty),\infty) = \phi_g$, where ϕ_∞ and $Z_c(\infty)$ are to be determined. The global conservation at equilibrium is:

$$\int_0^{Z_c(\infty)} \phi(Z, \infty) dZ = Z_f\phi_0 \tag{27}$$

Integrating Eq. 26 from 0 to $Z_c(\infty)$ gives ϕ_∞:

$$P_y(\phi_\infty) = Z_f\phi_0 \tag{28}$$

If $P_y(\phi)$ is given as an analytical function, the volume fraction distribution at equilibrium is determined explicitly by solving Eq. 26. However, to remain general, a 4th-5th order Runge-Kutta numerical technique is used here. Eq. 26 is integrated in 4th order steps of ΔZ from $\phi(0,\infty) = \phi_\infty$ until $\phi(Z,\infty) = \phi_g$. If a step gives $\phi < \phi_g$ or the error of the 5th order is outside a user-defined tolerance, ΔZ is reduced by a halving method. When $\phi = \phi_g$, $Z = Z_c(\infty)$.

Sedimentation Zone ($\phi_0 < \phi_g$, $Z_c(T) < Z < Z_s(T)$, $T \leq T_c$). For the $\phi_0 < \phi_g$ case, $\phi_s(T)$ and $Z_s(T)$ are determined independently of the consolidation zone. By definition, $\Delta(\phi) = 0$ for $\phi < \phi_g$. Thus, from Eq. 19, the solids flux in the settling zone, $\psi_s(Z,T)$, is given by:

$$\psi_s(Z, T) = (1 - Z)\frac{\phi_s}{B(\phi_s)}; \qquad Z_c(T) < Z < Z_s(T) \tag{29}$$

Differentiating with respect to Z and substituting into Eq. 20 gives:

$$\frac{\partial \phi_s}{\partial T} - (1 - Z)\left(\frac{\phi_s}{B(\phi_s)}\right)' \frac{\partial \phi_s}{\partial Z} = -\frac{\phi_s}{B(\phi_s)} \tag{30}$$

Equation 30 is a first-order nonlinear partial differential equation that is solved using the method of characteristics.[21] The solution depends on the functional form of $B(\phi)$ from $\phi_0 < \phi < \phi_g$, such that the discontinuity at $Z_c(T)$ can be a shock, a fan, or a combination of both.[6,18] The simplest scenario to consider involves a kinematic shock at $Z_c(T)$ (corresponding to Case Ia by Anestis and Schneider[6]). Since the coefficient of the first term is unity, Eq. 30 reduces to an ordinary differential equation, such that ϕ_s is independent of radius and is a function of time only:

$$\frac{d\phi_s}{dT} = -\frac{\phi_s}{B(\phi_s)} \tag{31}$$

The initial condition for this ordinary differential equation is $\phi_s(0) = \phi_0$. The volume fraction at $Z_s(T)$ is discontinuous. The velocity of the shock is[22]:

$$\frac{dZ_s}{dT} = -\frac{\psi_s(Z_s^+, T) - \psi(Z_s^-, T)}{\phi(Z_s^+, T) - \phi(Z_s^-, T)} = -\frac{(1 - Z_s)}{B(\phi_s)} \tag{32}$$

recognizing that ψ and ϕ are zero in the clear-liquor zone (at Z_s^+). Dividing Eq. 32 by Eq. 31 to eliminate T and integrating from $\phi_s(0) = \phi_0$ and $Z_s(0) = Z_f$ to $\phi_s(T)$ and $Z_s(T)$ gives an explicit relationship between $Z_s(T)$ and $\phi_s(T)$:

$$Z_s(T) = 1 - \frac{\phi_0}{\phi_s(T)}(1 - Z_f) \tag{33}$$

$Z_s(T)$ is dependent upon both Z_f and ϕ_0, such that, if the aim of the process is to clarify a liquid rather than consolidate a cake, low Z_f and ϕ_0 are preferable. As Z_f approaches unity (that is, the centrifuge is initially completely full of suspension), $Z_s(T)$ changes very little since the particles at the center of the centrifuge experience little or no acceleration.

At a theoretical time, T_s, the top of the sediment reaches the bowl wall, such that $Z_s(T_s) = 0$. T_s represents a limit for the solution of the sedimentation zone since it is always greater than T_c, the time when $Z_c(T) = Z_s(T)$.

$$\phi_s(T_s) = \phi_0(1 - Z_f) \tag{34}$$

Given an analytical function for $B(\phi)$, Eq. 31 can be solved explicitly. However, for the sake of generality, since $B(\phi)$ may be given as an interpolating or non-analytical function, it is solved here using the 4th-5th order Runge-Kutta numerical technique. Starting at $\phi_s(0) = \phi_0$, Eq. 31 is evaluated in 4th-order steps of ΔT. Z_s is evaluated at each time step using Eq. 33, and the process is repeated until $Z_s = 0$. If a step of ΔT gives a negative value for Z_s or the error of the 5th-order is too large, the step size is reduced using an interval halving method. The overall accuracy of the numerical method is checked by comparing the calculated ϕ_s value when $Z_s = 0$ with $\phi_s(T_s)$ from Eq. 34.

Consolidation Zone ($\phi_0 < \phi_g$, $0 < Z < Z_c(T)$, $T \le T_c$). A discontinuity in the volume fraction exists at $Z_c(T)$ in the initial suspension un-networked case. The velocity of the shock at $Z_c(T)$ is[22]:

$$\frac{dZ_c}{dT} = \frac{\psi_s(Z_c^+, T) - \psi(Z_c^-, T)}{\phi_g - \phi_s(T)}; \qquad T \le T_c \tag{35}$$

The global conservation equation for the un-networked case is:

$$Q(Z_c, T) + (Z_s - Z_c)\phi_s(T) = Z_f\phi_0; \qquad T \le T_c \tag{36}$$

$Q(Z,T)$ is the cumulative volume balance:

$$\frac{\partial Q}{\partial Z} = \phi \tag{37}$$

Due to the discontinuity at $Z_c(T)$, a change of variables to $X = Z/Z_c$ is made such that Eqs. 19 and 20 become:

$$\frac{\partial \phi}{\partial X} = -\frac{Z_c}{\Delta(\phi)}\left[\frac{\phi}{B(\phi)} - \frac{\psi}{1 - XZ_c}\right] \tag{38}$$

$$\frac{\partial \psi}{\partial X} = Z_c\frac{\partial \phi}{\partial T} - X\frac{dZ_c}{dT}\frac{\partial \phi}{\partial X} \tag{39}$$

A numerical method is used to solve the nonlinear partial differential equations that govern the behavior in the consolidation zone. A forwards difference approximation in time is made such that Eqs. 38 and 39 become ordinary differential equations for ϕ and ψ with respect to X at time T, which requires knowledge of the solution at the previous time step, $T - \Delta T$ (where ΔT is the size of the time step):

$$\frac{d\phi}{dX} = -\frac{Z_c}{\Delta(\phi)}\left[\frac{\phi}{B(\phi)} - \frac{\psi}{1 - XZ_c}\right] \tag{40}$$

$$\frac{d\psi}{dX} = Z_c\frac{\phi(X, T) - \phi(X, T - \Delta T)}{\Delta T} - X\frac{dZ_c}{dT}\frac{d\phi}{dX} \tag{41}$$

The numerical scheme involves taking fixed steps in the bowl wall volume fraction of size $\Delta\phi$. $\Delta\phi$ is chosen as the fixed variable rather than ΔT since $\phi(0,T)$ initially increases dramatically, as is shown later in the Results section. For each step, there are two unknown variables, ΔT^* and dZ_c^*/dT, which are solved iteratively using an interval halving technique. The upper and lower bounds for these variables (dZ_c/dT_{high}, dZ_c/dT_{low}, ΔT_{high}, and ΔT_{low}) for the first step are given by the small-time solution (given later). For the first iteration at each step, dZ_c^*/dT is well bounded by the result from the previous step, $dZ_c^</dT$, and 0. The lower initial bound of ΔT^* for each step is the previous result, $\Delta T^<$. However, the upper bound for ΔT^* is not well defined and is assumed here to be no more than twice the previous result. Z_c^* is approximated to order ΔT^3 for each value of ΔT^* and dZ_c^*/dT by the trapezium rule:

$$Z_c^*(T^*) = Z_c^< + \frac{\Delta T^*}{2}\left(\frac{dZ_c^*}{dT} + \frac{dZ_c^<}{dT}\right) \tag{42}$$

Equations 40 and 41 are solved from $X = 0$ (where $\phi(0,T^*) = \phi(0,T^<) + \Delta\phi$ and $\psi(0,T^*) = 0$) using the 4th-5th order Runge-Kutta technique until $\phi = \phi_g$, $d\phi/dX = 0$, or $X = 1$. If $\phi(X,T^*) = \phi_g$ for $X < 1$, ΔT^* is too large and becomes the new upper bound for ΔT. If $\phi(1,T^*) > \phi_g$ or $d\phi/dX = 0$, ΔT^* is too small and becomes the new lower bound for ΔT. ΔT^* is iterated upon until $\phi(1,T^*) = \phi_g$. $\psi(1,T^*)$ is then used in Eq. 35 to give an iteration test value for dZ_c/dT, dZ_c/dT_{test}:

$$\frac{dZ_c}{dT_{test}} = \frac{\psi_s(Z_c^*, T^*) - \psi(1, T^*)}{\phi_g - \phi_s(T^*)} \tag{43}$$

If $dZ_c^*/dT > dZ_c/dT_{test}$, dZ_c^*/dT is too high and becomes the new upper bound for dZ_c/dT. If $dZ_c^*/dT < dZ_c/dT_{test}$, then the estimate is too low and becomes the new lower bound for dZ_c/dT. dZ_c^*/dT is iterated upon until it is equal to the test value to the desired precision. For each iteration of dZ_c^*/dT, ΔT^* must be re-evaluated. By evaluating $Q(Z,T)$ with each step, Eq. 36 gives a check on the accuracy of the iterative numerical technique at each time step.

Once a time step gives a result of $Z_c(T) \geq Z_s(T)$, $\Delta\phi$ is halved (and the initial upper and lower bounds for the iteration variables appropriately adjusted) and the algorithm is repeated until $Z_c(T_c) = Z_s(T_c)$ to the desired accuracy. Likewise, the accuracy of the algorithm decreases as ΔT increases. Therefore, if $\Delta T > \Delta T_{max}$, $\Delta\phi$ is halved for the next step. ΔT_{max} is chosen as 0.01.

Consolidation Zone ($\phi_0 < \phi_g$, $0 < Z < Z_c(T)$, $T > T_c$). After T_c, $Z_c(T)$ decreases since there is no material being added to the consolidating cake. The top of the cake remains at ϕ_g since there are no compressive forces to increase the concentration. The velocity of the shock at Z_c is given by setting $\phi_s = \psi_s = 0$ in Eq. 35:

$$\frac{dZ_c}{dT} = -\frac{\psi(Z_c^-, T)}{\phi_g}; \qquad T > T_c \tag{44}$$

The global solids conservation equation when there is no sedimentation zone is:

$$Q(Z_c, T) = Z_f\phi_0; \qquad T > T_c \tag{45}$$

There is no need to make the change of variables to X since Z_c is decreasing and $\phi(Z,T)$ exists for $Z_c^< < Z < Z_c(T)$. A forwards difference approximation in time is used to convert Eqs. 19 and 20 to two coupled ordinary differential equations of ϕ and ψ with respect to Z:

$$\frac{d\phi}{dZ} = -\frac{1}{\Delta(\phi)}\left[\frac{\phi}{B(\phi)} - \frac{\psi}{1-Z}\right] \tag{46}$$

$$\frac{d\psi}{dZ} = \frac{\phi(Z, T) - \phi(Z, T - \Delta T)}{\Delta T} \tag{47}$$

For a given step of ΔT, there is one unknown, $\Delta\phi^*$, which is solved using an interval halving iterative approach. Rather than fixing $\Delta\phi$ and iterating on ΔT^* as in the previous scheme, ΔT is fixed in this formulation since $\Delta\phi^*$ is well bounded. The initial upper and lower bounds for $\Delta\phi^*$ at each time step are $(\phi_\infty - \phi^<(0))$ and 0, respectively.

The convergence of the iteration is based on the overall solids conservation. Eqs. 37, 46, and 47 are solved from $Z = 0$ (where $\phi(0,T) = \phi^<(0) + \Delta\phi^*$, and $\psi(0,T) = Q(0,T) = 0$) until $\phi = \phi_g$, $d\phi/dZ = 0$, or $Q = Z_f\phi_0$. If $\phi > \phi_g$, $\Delta\phi^*$ is too large. If $Q < Z_f\phi_0$, $\Delta\phi^*$ is too small. $\Delta\phi^*$ is iterated until $Q = Z_f\phi_0$ to the desired precision. The accuracy of the numerical scheme is given by comparing Eq. 44 with the trapezoidal approximation of dZ_c/dT (see Eq. 42).

Analytical Similarity Series Solution for Small Times ($\phi_0 < \phi_g$, $T \ll 1$). The height of the consolidating bed and the volume fraction at the bowl wall for small times are given by the leading order terms of the analytical similarity series solution, which are presented here without derivation:

$$Z_c(T) = \frac{\phi_0}{(\phi_g - \phi_0)}T; \qquad T \ll 1 \tag{48}$$

$$\phi(0, T) = \phi_g\left[1 + \frac{\phi_0}{(\phi_g - \phi_0)}\frac{T}{P_y'(\phi_g)}\right]; \qquad T \ll 1 \tag{49}$$

Interestingly, Z_c varies linearly with T to leading order. This occurs with pressure filtration with membrane resistance,[14] whereas for batch settling[8] and pressure filtration without membrane resistance,[13] the asymptotic results for Z_c vary with $\sqrt{T}$. Equations 48 and 49 are used to give the bounds for the first step in the algorithm.

Case 2: initial suspension networked ($\phi_0 > \phi_g$)

Unlike the $\phi_0 < \phi_g$ case, the solution in the sedimentation zone for the $\phi_0 > \phi_g$ case is coupled with the consolidation zone results, since $\phi(Z_c,T)$ and $\psi(Z_c,T)$ are continuous.

Sedimentation Zone ($\phi_0 > \phi_g$, $Z_c(T) < Z < Z_s(T)$). The suspension slumps at constant concentration, $\phi_s = \phi_0$, in the sedimentation zone since $p_p < p_y(\phi)$. Therefore, from Eq. 20, the gradient of the solids flux is zero and ψ_s is constant with respect to Z. The pressure gradient is given by Eq. 22. Substituting ϕ_0 and ψ_s gives the pressure gradient in the sedimentation zone:

$$\frac{\partial P_p}{\partial Z} = \frac{\psi_s}{1 - Z} - \phi_0 \tag{50}$$

Integrating Eq. 50 from $P_p(Z_c,T) = P_y(\phi_0)$ to $P_p(Z_s,T) = 0$ gives the relationship between Z_c and Z_s:

$$P_y(\phi_0) = \psi_s\ln\left(\frac{1 - Z_s}{1 - Z_c}\right) + \phi_0(Z_s - Z_c) \tag{51}$$

The global solids conservation equation for the $\phi_0 > \phi_g$ case is:

Table 1. Material Parameters for Ferric Water Treatment Sludge

Parameter	Value
p_1 (Pa)	7.1836
p_2	3.1142
ϕ_g (v/v)	0.0040
r_1 (Pas/m^2)	5.10×10^{13}
r_2	−17.3077
$\Delta\rho$ (kg/m^3)	3000

$$\int_0^{Z_c} \phi dZ + (Z_s - Z_c)\phi_0 = Z_f\phi_0 \tag{52}$$

Eliminating Z_s from Eqs. 51 and 52 and substituting $Q_c = Q(Z_c,T)$ gives:

$$P_y(\phi_0) = \psi_s \ln\left(1 - \frac{Z_f\phi_0 - Q_c}{\phi_0(1 - Z_c(T))}\right) + Z_f\phi_0 - Q_c \tag{53}$$

Equation 53 couples the consolidation and sedimentation zones, since ψ_s equals $\psi(Z_c^-,T)$. The velocity of the shock at $Z_s(T)$ is given by[22]:

$$\frac{dZ_s}{dT} = -\frac{\psi_s}{\phi_0} \tag{54}$$

Equilibrium Solution ($\phi_0 > \phi_g$, $T\to\infty$). As $T \to \infty$, the sedimentation zone will not disappear for the $\phi_0 > \phi_g$ case since there will always be material above the cake where the compressive forces acting upon the network are less than the strength of the network. Setting $\psi = 0$ in Eq. 51 gives the relationship between $Z_s(\infty)$ and $Z_c(\infty)$:

$$Z_s^\infty = \frac{P_y(\phi_0)}{\phi_0} + Z_c^\infty \tag{55}$$

Setting $\psi = 0$ in Eq. 22 gives the particle pressure gradient throughout the suspension at equilibrium:

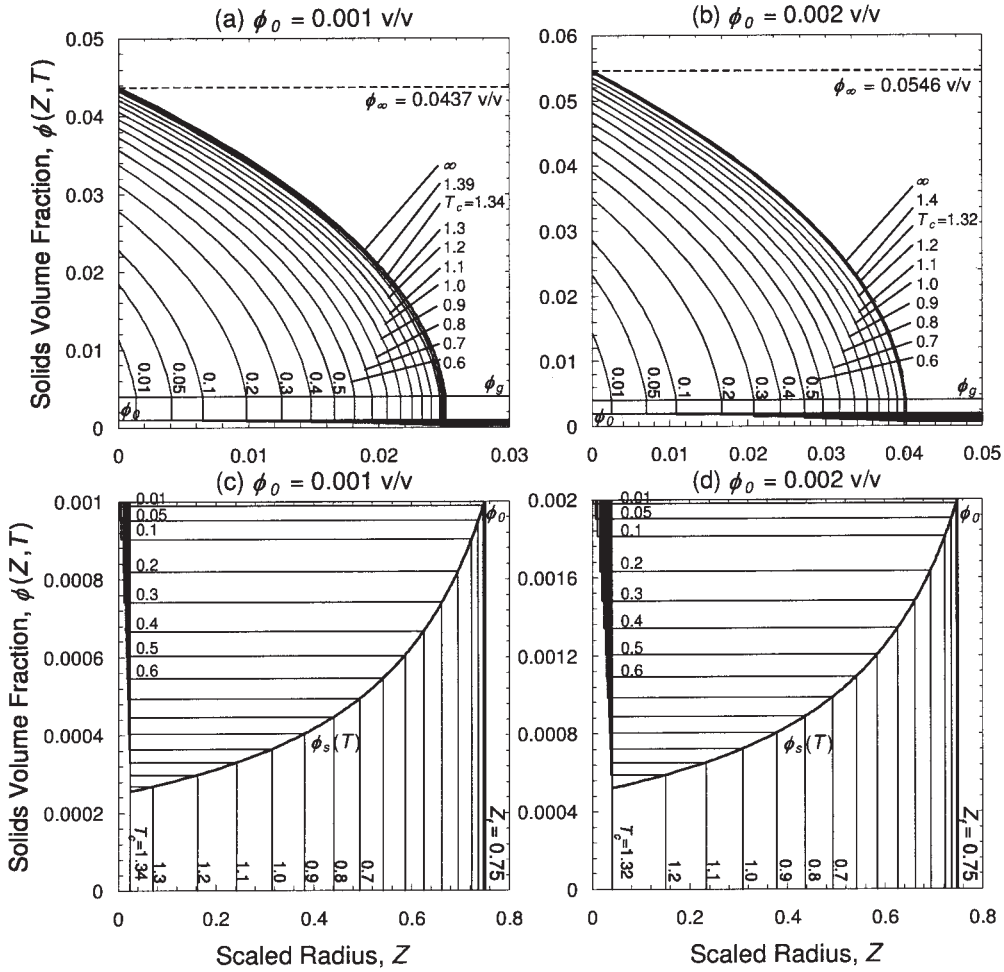

Figure 2. Volume fraction distribution predictions for batch centrifuge model with different initial concentrations ($\phi_o < \phi_g$, rb = 0.5 m, rf = 0.25 m, and ω = 2000 rpm).

The annotated values correspond to scaled times. (c) and (d) are enlarged views of (a) and (b).

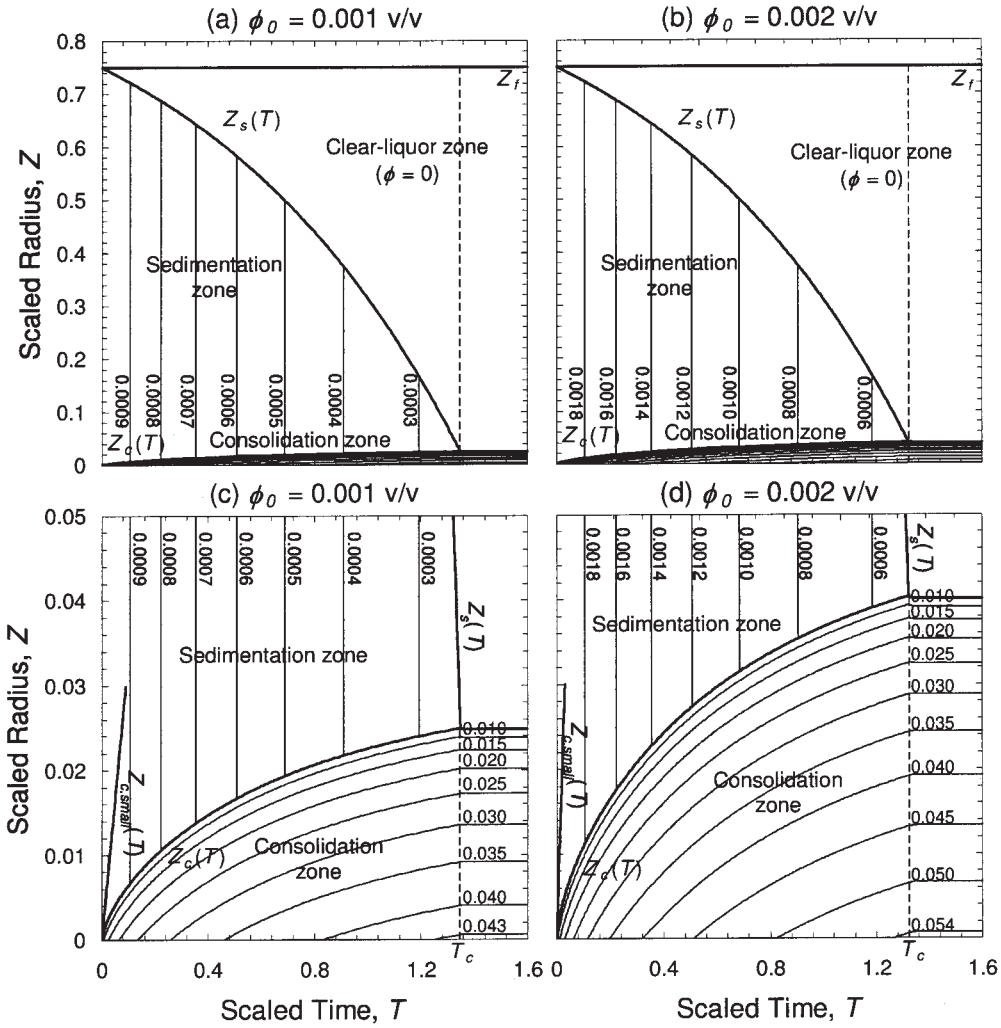

Figure 3. Predictions of sedimentation and consolidation profiles for batch centrifuge model with differing initial concentrations ($\phi_0 < \phi_g$, rb = 0.5 m, r_f = 0.25 m, and ω = 2000 rpm).

The annotated values correspond to lines of constant concentration. (c) and (d) are enlarged views of (a) and (b).

$$\frac{dP_p}{dZ} = -\phi \tag{56}$$

Integrating Eq. 56 from $P_p(0) = P_y(\phi_\infty)$ to $P_p(Z_s(\infty)) = 0$ yields Eq. 28 as previously. $\phi(Z,\infty)$ in the consolidation zone is given by solving Eq. 26 from $\phi(0,\infty) = f\infty$ until $\phi(Z_c(\infty),\infty) = \phi_0$. $Z_s(\infty)$ is then given by Eq. 55.

Consolidation Zone ($\phi_0 > \phi_g$, $0 < Z < Z_c(T)$. $\phi(Z,T)$ in the consolidation zone is given by Eqs. 46 and 47. For a given step of $\Delta\phi$ (typically chosen as 0.01 ($\phi_\infty - \phi_0$)), there is one unknown, ΔT^*, which is solved using an interval halving iterative approach. The small-time solution, which is derived later, gives the upper and lower bounds for ΔT^* (ΔT_{high} and ΔT_{low}) for the first step. The initial lower bound for ΔT^* for each subsequent step is the value from the previous step, $\Delta T^<$ (providing that $\Delta\phi$ is constant), while the initial upper bound for ΔT^* for each step is chosen as 2 $\Delta T^<$.

Equations 37, 46, and 47 are solved from $Z = 0$ (where $\phi(0,T) = \phi^<(0) + \Delta\phi$, and $\psi(0,T) = Q(0,T) = 0$) until $\phi(Z,T) = \phi_0$ or $d\phi/dZ = 0$. If the latter condition is met and $\phi(Z,T) > \phi_0$, ΔT^* is too small. If $\phi(Z,T) = \phi_0$, the right-hand side of Eq. 53 is evaluated using Z, $\psi(Z,T)$, and $Q(Z,T)$. If the solution is less than $P_y(\phi_0)$, ΔT^* is too small, whereas if the solution is greater than $P_y(\phi_0)$, ΔT^* is too large. ΔT^* is iterated until Eq. 53 is obeyed to the required precision. The accuracy of the numerical solution is indicated by evaluating ψ_s from Eq. 54 using an appropriate approximation to dZ_s/dT and comparing to $\psi_c(Z_c^-,T)$.

Analytical Similarity Series Solution for Small Times ($\phi_0 > \phi_g$, $T \ll 1$). The following asymptotic results hold for $Z_s(T)$, $Z_c(T)$, and $\phi(0,T)$:

$$Z_s(T) = Z_f - \lambda T \tag{57}$$

$$Z_c(T) = 2A\sqrt{P_y'(\phi_0)T} \tag{58}$$

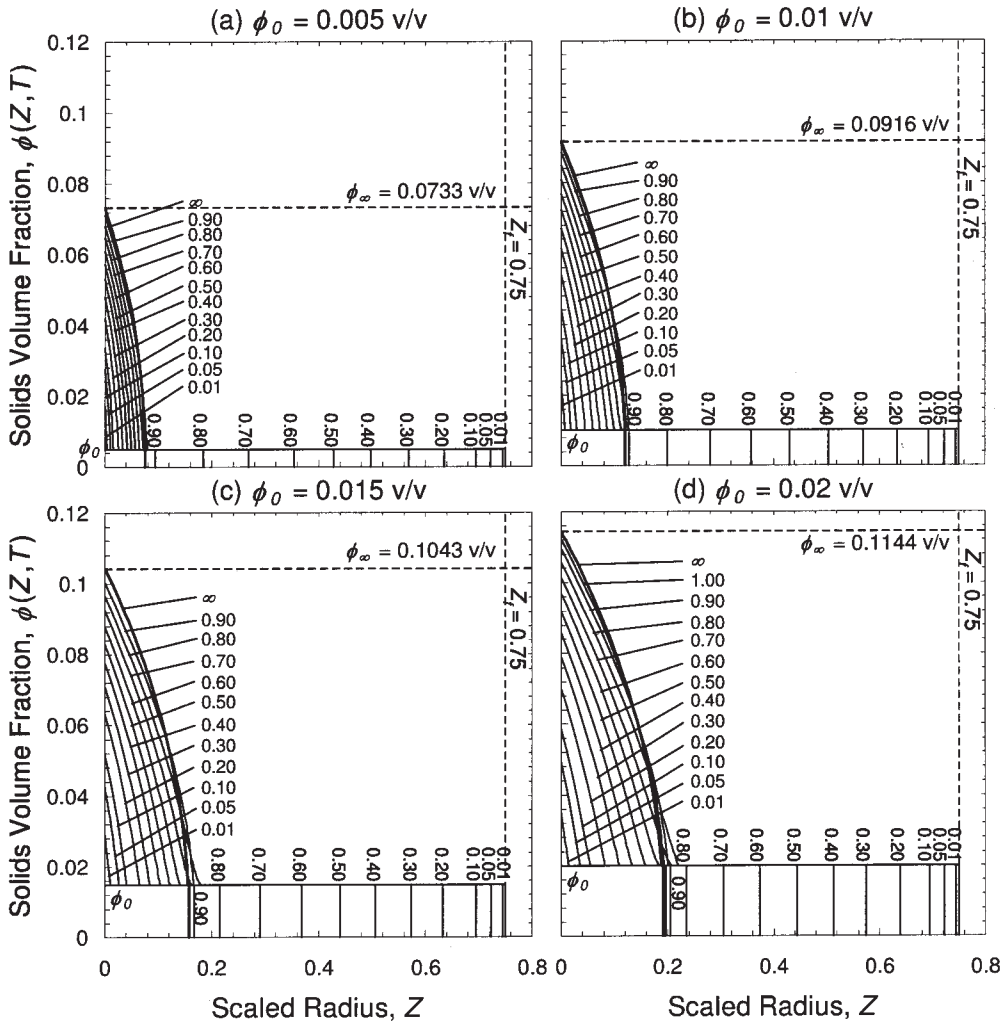

Figure 4. Volume fraction distribution predictions for batch centrifuge model with different initial concentrations ($\phi_o > \phi_g$, rb = 0.5 m, r_f = 0.25 m, and ω = 2000 rpm).

The annotated values correspond to scaled times.

$$\phi(0, T) = \phi_0\left[1 + \sqrt{T}\,\frac{2Ae^{A^2}(1-\lambda)}{\sqrt{P_y'(\phi_0)}}\right] \tag{59}$$

where A is the solution to:

$$\sqrt{\pi}\,Ae^{A^2}\mathrm{erf}\,A = \frac{\lambda}{1-\lambda} \tag{60}$$

and λ is given by:

$$\lambda = \frac{P_y(\phi_0) - \phi_0 Z_f}{\phi_0 \ln(1 - Z_f)} \tag{61}$$

The small time behavior for Z_c varies with $\sqrt{T}$ rather than T. Thus, all the time derivatives tend to infinity as $T \to 0$.

Modeling Results

Typically, power-law functions of the following type are used to represent $p_y(\phi)$ and $R(\phi)$[12,23-30]:

$$p_y(\phi) = \begin{Bmatrix} 0 & \phi < \phi_g \\ p_1\left[\left(\dfrac{\phi}{\phi_g}\right)^{p_2} - 1\right] & \phi \geq \phi_g \end{Bmatrix} \tag{62}$$

$$R(\phi) = r_1(1-\phi)^{r_2} \tag{63}$$

The parameters for Eqs. 62 and 63 for a ferric water treatment sludge[31] are given in Table 1. These material characteristics were measured by stepped-pressure filtration testing over a volume fraction range from 0.04 to 0.16 v/v. ϕ_g was measured using equilibrium batch settling to be 0.004 v/v.

These material properties are used here to illustrate the batch centrifuge models. The material characteristics are extrapolated using the fitted power-law functional forms for $R(\phi)$ values below ϕ_g and, therefore, represent a simplistic case where the solution to Eq. 30 is always a shock at $Z_c(T)$. The results for fixed operating conditions (r_b = 0.5 m, r_f = 0.25 m, and ω = 2000 rpm) with a range of initial concentrations (above and below ϕ_g) are investigated.

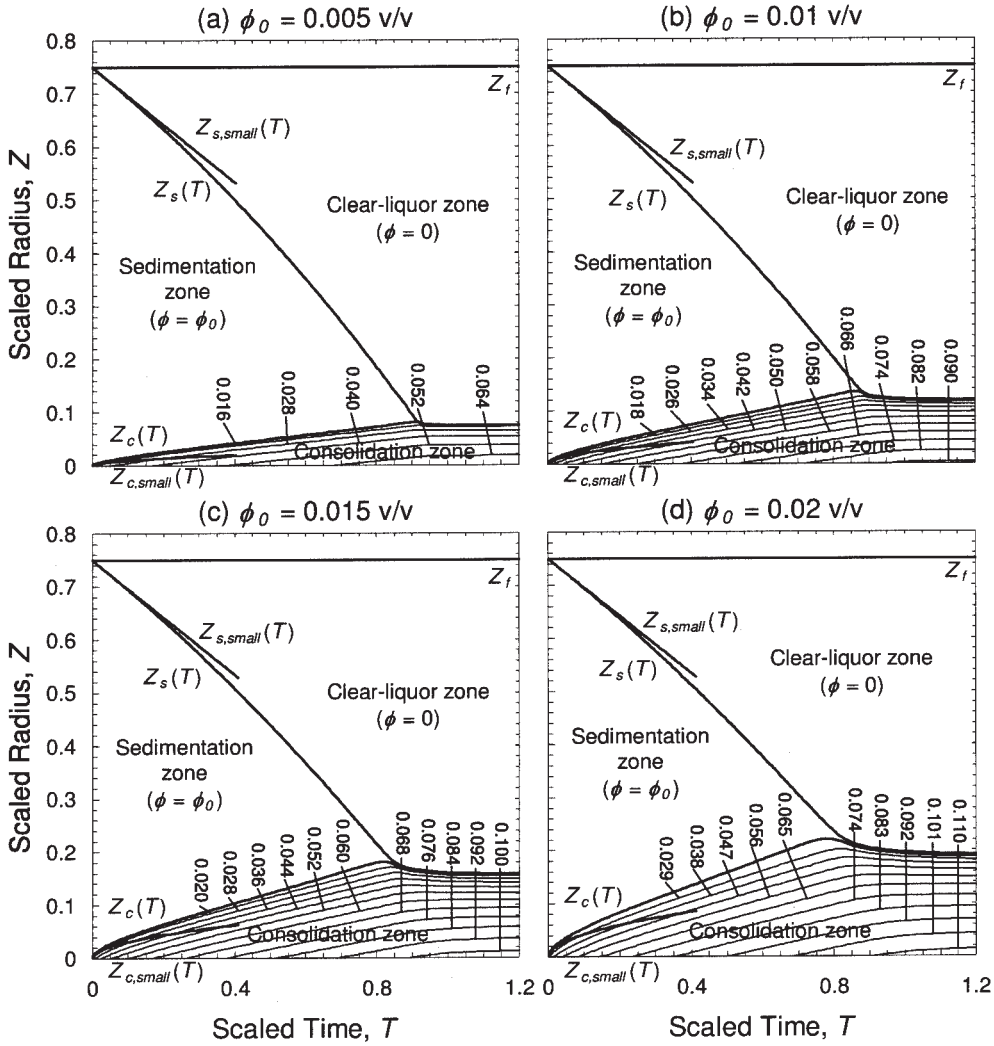

Figure 5. Predictions of sedimentation and consolidation profiles for batch centrifuge model with differing initial concentrations ($\phi_O > \phi_g$, r_b = 0.5 m, r_f = 0.25 m, and ω = 2000 rpm).

The annotated values correspond to lines of constant concentration.

Case 1: Initial suspension un-networked ($\phi_0 < \phi_g$)

Figure 2 shows the volume fraction distribution results for the batch centrifuge model with $\phi_0 = 0.001$ and 0.002 v/v, such that the initial suspension is un-networked. The results illustrate the build-up of the cake (2a and 2b) and the decrease of the sediment volume fraction with time (2c and 2d). The concentration jumps from ϕ_s to ϕ_g at the cake/sediment interface.

As T approaches and passes T_c, the cake concentration approaches the equilibrium distribution, indicating that the transient numerical solution is valid. There are only very small changes in ϕ after T_c, such that the sedimentation time-scale is greater than the consolidation time-scale.

The concentration profile results for $\phi_0 = 0.001$ and 0.002 v/v are presented in Figures 3a and 3b, with enlarged views of the consolidation zone in 3c and 3d, respectively. For these material characteristics and operating conditions, ϕ_s is a function of T but independent of Z. The enlarged views show that the small time approximation over-predicts $Z_c(T)$ and applies only for very small values of T, and further illustrate the small changes in concentration after T_c.

Case 2: Initial suspension networked ($\phi_0 > \phi_g$)

Figure 4 shows the volume fraction distribution results for $\phi_0 > \phi_g$. ϕ is initially constant throughout the centrifuge at ϕ_0. With the onset of centrifugal acceleration, $\phi(0,T)$ increases dramatically as the solids sediment from the liquid to form the cake. $Z_c(T)$ passes through a maximum and begins to decrease since the acceleration is a function of radius. As ϕ_0 is increased, the final height and equilibrium concentration increase.

$\phi(Z,T)$ approaches the equilibrium distribution as T increases, indicating that the numerical algorithm is valid. ϕ_s is constant at ϕ_0 throughout the process. The maximum in $Z_c(T)$ becomes more pronounced as ϕ_0 is increased, since the consolidation time-scale increases compared to the sedimentation time-scale.

The concentration profile results for the networked case are

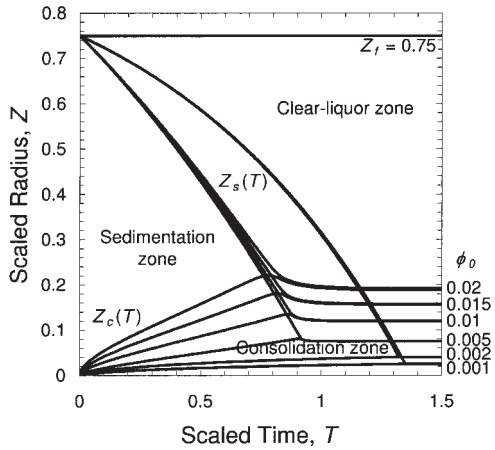

Figure 6. Transient sediment and cake height results for batch centrifuge model with different initial concentrations (r_b = 0.5 m, r_f = 0.25 m, and ω = 2000 rpm).

presented in Figure 5. The small time approximations for $Z_c(T)$ are less than the numerical solutions and apply for T values up to 0.1. $Z_{s,small}(T)$ is greater than the numerical solution, and is accurate up to considerable values of T. These results represent the first reported modeling of the initial suspension networked case of batch centrifugation.

The transient sediment and cake height results are presented in Figure 6, which clearly shows the change in behavior of the sedimentation zone between the networked and un-networked cases. Since the time scaling is based on ϕ_0, the $Z_s(T)$ results within each case are initially equal. However, for the $\phi_0 > \phi_g$ case, $Z_s(T)$ is initially linear, while it is non-linear for the $\phi_0 < \phi_g$ case. Figure 6 also shows the increasing cake height with increasing ϕ_0.

The equilibrium distribution results are presented in Figure 7. The sedimentation zone does not exist and the top of the cake is at ϕ_g for the $\phi_0 < \phi_g$ case, whereas the sediment is present and at ϕ_0 for the $\phi_0 > \phi_g$ case. As ϕ_0 is increased, ϕ_∞ increases since the solids pressure at the bowl wall increases, and $Z_{c\infty}$ increases since the total amount of solids increases. Thus, in general, high solids loadings are necessary to achieve high cake concentrations in centrifugal operations.

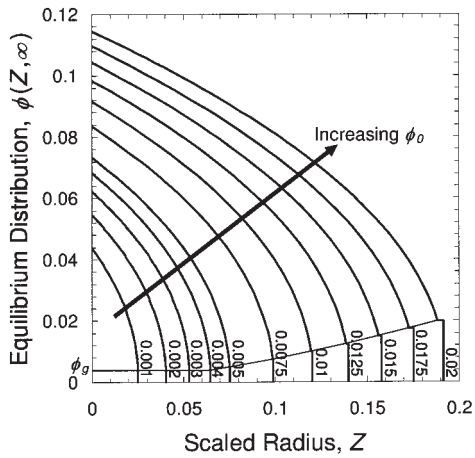

Figure 7. Equilibrium volume fraction distribution results for one-dimensional batch centrifuge model with different initial concentrations (r_b = 0.5 m, r_f = 0.25 m, and ω = 2000 rpm).

The models can also be used to investigate the effect of changes to other operating parameters, centrifuge dimensions, and/or material properties.

Conclusions

Models of solid-bowl batch centrifugation of flocculated suspensions are formulated for the two cases of initial suspension networked and un-networked and solved using Runge-Kutta numerical techniques. The algorithms are generalized such that any material property functional forms can be used. The models are illustrated using the material characteristics of a ferric water treatment sludge. The results show that three zones of behavior exist: a clear liquor zone from which material has settled, a sedimentation zone, and a consolidation zone as cake builds up from the wall of the centrifuge. The volume fraction distribution in the settling zone is shown to be constant with respect to radius but changing with time for the initial suspension un-networked case, and constant for the initial suspension networked case. The models can be used for prediction, optimization, and design purposes.

Acknowledgments

Financial support for this work was through the Particulate Fluids Processing Centre, a Special Research Centre of the Australian Research Council. Industrial sponsorship from United Utilities PLC, United Kingdom, and Yorkshire Water Services Ltd, United Kingdom, is also acknowledged.

Notation

Latin alphabet

A = small-time coefficient ($\phi_0 > \phi_g$)
$B(\phi)$ = scaled hindered settling function
$\mathbf{g}$ = acceleration vector (m^2/s)
$p_p(r,t)$ = local particle pressure (Pa)
$p_y(\phi)$ = compressive yield stress (Pa)
p_1, p_2 = compressive yield stress power-law parameters
$P_p(Z,T)$ = scaled particle pressure
$P_y(\phi)$ = scaled compressive yield stress
$Q(Z,T)$ = scaled cumulative solids volume
r = radial coordinate (m)
r_1, r_2 = hindered settling function power-law parameters
$R(\phi)$ = hindered settling function (Pas/m^2)
t = time (s)
t_c = critical time for sediment to disappear (s)
T = scaled time
T_c = scaled time for sediment to disappear ($\phi_0 < \phi_g$)
T_s = theoretical scaled time when $Z_s = 0$ ($\phi_0 < \phi_g$)
$\mathbf{u}$, $u(r,t)$ = local particle velocity (m/s)
V_0 = initial suspension volume per unit length (m^3/m)
$\mathbf{w}$, $w(r,t)$ = local fluid velocity (m/s)
X = scaled radial coordinate
Z = scaled radial coordinate

Greek letters

$\Delta\rho$ = density difference between solid and liquid phases (kg/m^3)
$\Delta(\phi)$ = scaled solids diffusivity
$\Delta\phi$ = change in ϕ_b *for a given* ΔT
ΔT = scaled time step
$\phi(r,t)$ = local solids volume fraction (v/v)
ϕ_∞ = bowl wall solids volume fraction at equilibrium (v/v)

ϕ_0 = initial solids volume fraction (v/v)
ϕ_g = gel point solids volume fraction (v/v)
$\kappa(\phi)$ = dynamic compressibility ((Pa.s)$^{-1}$)
λ = small-time coefficient ($\phi_0 > \phi_g$)
ω = angular velocity (rad/s)
$\psi(Z,T)$ = scaled local solids flux

Subscripts and superscripts

b = bowl
c = cake/consolidation zone
f = fluid/liquid
p = particle/solid
s = sediment/sedimentation zone
high/low = upper and lower bounds for iteration variable
test = test value for iteration variable
∞ = equilibrium solution
+/- = upper and lower limit values for discontinuity
* = estimate for iteration variable
< = result from previous time step

Literature Cited

1. Ambler CM. The evaluation of centrifuge performance. *Chem Eng Progr.* 1952;48(3):150-157.
2. Ambler CM. The theory of scaling up laboratory data for the sedimentation type centrifuge. *J Biochem Micro Tech Eng.* 1959;1(2):185-205.
3. Tiller FM, Shirato M. The role of porosity in filtration: VI. New definition of filtration resistance. *AIChE J.* 1964;10(1):61-67.
4. Tiller FM, Hsyung NB. Unifying the theory of thickening, filtration, and centrifugation. *Wat Sci Tech.* 1993;28(1):1-9.
5. Corner-Walker N. The dry solids decanter centrifuge: capacity scaling. *Filtr Sep.* 2000;37(4):28-32.
6. Anestis G, Schneider W. Application of the theory of kinematic waves to the centrifugation of suspensions. *Ing-Arch.* 1983;53:399-407.
7. Kynch GJ. A theory of sedimentation. *Trans Faraday Soc.* 1952;48:166-176.
8. Buscall R, White LR. The consolidation of concentrated suspensions. Part 1. The theory of sedimentation. *J Chem Soc, Faraday Trans.* 1. 1987;83:873-891.
9. Green MD, Eberl M, Landman KA. Compressive yield stress of flocculated suspensions: determination via experiment. *AIChE J.* 1996;42(8):2308-2318.
10. Howells I, Landman KA, Panjkov A, Sirakoff C, White LR. Time dependent batch settling of flocculated suspensions. *Appl Math Model.* 1990;14:77-86.
11. Landman KA, White LR, Buscall R. The continuous flow gravity thickener: steady state behaviour. *AIChE J.* 1988;34(2):239-252.
12. Landman KA, White LR. Solid/liquid separation of flocculated suspensions. *Adv Colloid Interface Sci.* 1994;51:175-246.
13. Landman KA, White LR. Predicting filtration time and maximizing throughput in a pressure filter. *AIChE J.* 1997;43(12):3147-3160.
14. Landman KA, Sirakoff C, White LR. Dewatering of flocculated suspensions by pressure filtration. *Phys Fluids A.* 1991;3(6):1495-1509.
15. Martin AD. Filtration of flocculated suspensions under declining pressure. *AIChE J.* 2004;50(7):1418-1430.
16. de Kretser RG, Usher SP, Scales PJ, Boger DV, Landman KA. Rapid filtration measurement of dewatering design and optimisation parameters. *AIChE J.* 2001;47(8):1758-1769.
17. Lester DR, Usher SP, Scales PJ. Estimation of the hindered settling function R(ϕ) from batch settling tests. *AIChE J.* 2005;51(4):1158-1168.
18. Bürger R, Concha F. Settling velocities of particulate systems: 12. Batch centrifugation of flocculated suspensions. *Int J Miner Process.* 2001;63:115-145.
19. Barr JD, White LR. Centrifugal drum filtration (I): A compression rheology model of cake formation. *AIChE J.* 2005;in press.
20. Barr JD, White LR. Centrifugal drum filtration (II): A compression rheology model of cake draining. *AIChE J.* 2005;in press.
21. Hildebrand FB. *Methods of Applied Mathematics*. 1st ed. Englewood Cliffs, NJ: Prentice-Hall; 1952:523.
22. John F. *Partial Differential Equations*. 4th ed. New York: Springer-Verlag; 1982.
23. Buscall R, Mills PDA, Stewart RF, Sutton D, White LR, Yates GE. The rheology of strongly-flocculated suspensions. *J Non-Newtonian Fluid Mech.* 1987;24(2):183-202.
24. Auzerais FM, Jackson R, Russel WB, Murphy WF. The transient settling of stable and flocculated dispersions. *J Fluid Mech.* 1990;221:613-639.
25. Channell GM, Zukoski CF. Shear and compressive rheology of aggregated alumina suspensions. *AIChE J.* 1997;43(7):1700-1708.
26. Eberl M, Landman KA, Scales PJ. Scale up procedures and test methods in filtration: a test case on kaolin plant data. *Colloids Surf A.* 1995;103:1-10.
27. Eckert WF, Masliyah JH, Gray MR, Fedorak PM. Prediction of sedimentation and consolidation of fine tails. *AIChE J.* 1996;42(4):960-972.
28. Green MD, Boger DV. Yielding of suspensions in compression. *Ind Eng Chem Res.* 1997;36:4984-4992.
29. Miller KT, Melant RM, Zukoski CF. Comparison of the compressive yield response of aggregated suspensions: pressure filtration, centrifugation, and osmotic consolidation. *J Am Ceram Soc.* 1996;79(10):2545-2556.
30. Tiller FM, Khatib Z. Theory of sediment volumes of compressible, particulate structures. *J Colloid Interface Sci.* 1984;100(1):55-67.
31. Harbour PJ, Anderson NJ, Abd Aziz AA, Dixon DR, Hillis P, Scales PJ, Stickland AD, Tillotson M. Fundamental dewatering characteristics of potable water treatment sludges. *J Wat Supply: Res Tech–Aqua.* 2004;53(1):29-36.

Manuscript received May 24, 2005, and revision received Nov. 6, 2005.